Fotogrametrični poligon za zajem podatkov v zaprtih prostorih

Photogrammetric traverse for indoor positioning

Klemen Kozmus Trajkovski, Tilen Urbančič, Bojan Stopar, Dejan Grigillo

UDK: 528.74:72.012.8
Klasifikacija prispevka po COBISS.SI: 1.01
Prispelo: 30. 12. 2024
Sprejeto: 30. 4. 2025

DOI: 10.15292/geodetski-vestnik.2025.02.148-179
SCIENTIFIC ARTICLE
Received: 30. 12. 2024
Accepted: 30. 4. 2025

IZVLEČEK

Prispevek predstavlja uporabo fotogrametričnih poligonov za orientacijo fotografij za namen masovnega zajema prostorskih podatkov na območjih, kjer izmera z GNSS (angl. global navigation satellite systems) ali tahimetrična izmera nista mogoči ali nista zanesljivi, na primer v notranjosti stavb. Fotogrametrične poligone smo preskusili v notranjosti stavbe. Osnovno načelo fotogrametričnega poligona je njegov začetek na območju, kjer izmerimo položaje oslonilnih točk. Temu sledi zajem serije fotografij, ki se med seboj prekrivajo in s katerimi razvijemo fotogrametrični poligon. Orientacijo fotografij in točnost določitve položaja točk vzdolž poligona ocenimo s postopkom grajenja strukture iz gibanja (angl. structure from motion). Preizkusili in analizirali smo odprt, priklepni in zaključeni fotogrametrični poligon. Položajna točnost kontrolnih točk je bila v mejah 10 centimetrov, tudi pri obdelavi več sto fotografij v najmanj natančnem odprtem poligonu.

ABSTRACT

The article presents the use of photogrammetric traverses for image orientation and the acquisition of mass spatial data in environments where GNSS (Global Navigation Satellite Systems) or tachymetric surveys are not available or not reliable, such as inside buildings. The photogrammetric traverses were tested indoors. The basic idea of a photogrammetric traverse is to start from an area where the positions of the ground control points are surveyed and then use a still camera to develop a traverse of overlapping images. The images are then processed with SfM (Structure from Motion) to calculate their orientation and accuracy of points along the traverse. The study tested the accuracy and reliability of linked, looped and open photogrammetric traverses. The positional accuracy of the check points was better than 10 cm, even when adjusting several hundred images in the least accurate open traverse.

KLJUČNE BESEDE

fotogrametrija, določanje položaja, izmera, poligon, grajenje strukture iz gibanja, masovni zajem prostorskih podatkov

KEY WORDS

photogrammetry, positioning, survey, traverse, Structure from Motion, mass spatial data acquisition

1 INTRODUCTION

The importance of the study lies in an innovative way of mass positioning that combines principles of classical terrestrial traverse positioning and photogrammetry. The common surveying methods are tachymetry and GNSS positioning. Both offer high-precision positioning down to the millimeter, as Wang (2013) states, whereby the positions are only determined point by point with both methods. The acquisition of spatial mass data along a traverse is also possible with TLS (Terrestrial Laser Scanning) and MMS (Mobile Mapping System). The photogrammetric traverse is presented as an alternative to the portable MMS, which can be held in the hand or positioned on a trolley. This system is a much more expensive investment than a common photo camera. Photogrammetric traverse is much faster in the field than TLS, also noted in Nadal-Romero et al. (2015). However, it requires a little more work in the office.

A traverse survey is used when the network of known reference points needs to be extended to an area without reference points. During the survey, tachymetry is used to extend the network of points from the reference points to other reference points (linked traverses), back to the same reference points (looped traverses) or to new points (open traverses). Linked and looped traverses allow for high-quality positioning, while there is no real quality control with the open traverse.

In this article, we present all three types of traverses (linked, looped and open) extended with sequences of overlapping images and processed with Structure from Motion (SfM). SfM uses multiple highly overlapping images and image matching algorithms to simultaneously determine interior and exterior camera parameters and reconstruct the 3D scene in the form of a sparse point cloud, according to Rupnik, Daakir and Pierrot Deseilligny (2017), Carrivick, Smith and Quincey (2016), Westoby et al. (2012), and Barazzetti, Scaioni and Remondino (2010). In a critical review of dense image matching algorithms (Remondino et al., 2014), SfM tools are categorized in the black box category where divergence in bundle adjustment or geometric deformations may occur. It is therefore necessary to include the image coordinates of the GCPs (Ground Control Points) in the image block adjustment. GCPs are precisely measured in the object coordinate system and are usually signalized with targets that enable automatic measurement of their image coordinates. Special attention must also be paid to camera self-calibration, which is included in SfM. Barazzetti et al. (2012) and Micheletti, Chandler and Lane (2015a) state that the image block should contain convergent, multiscale and rotated images to strengthen the geometry for calculating the interior orientation in the process of self-calibration. Sufficient variation in scale within the imagery support the reliable recovery of the camera interior orientation parameters (Luhmann Fraser and Maas, 2016).

To obtain reliable metric information and evaluate the accuracy of the results, we set a network of signalized GCPs at the beginning, along the traverse and at the end to georeference the point cloud obtained from the images. The accuracy of the methods was evaluated based on the coordinate differences at the numerous check points (CPs) measured along the traverses. Surveying techniques such as tachymetry or GNSS positioning are used to determine accurate positions of the GCPs and CPs. In contrast to point positioning with tachymetry or GNSS, the photogrammetric traverse provides mass positioning with millions of points when the dense point cloud is calculated from oriented images. The dense point cloud is generated with dense image matching algorithms, usually with MVS (Multi-View Stereo), as described in Furukawa and Hernández (2015).

Similar techniques have been widely used to bridge GNSS outages when processing MMS (Mobile Mapping System) data, whether terrestrial (Silva, Lemes Neto and Blasechi (2014) and Roncella, Remondino and Forlani (2005)) or UAV-based (Elbahnasawy et al., 2018). These methods are often referred to as photogrammetric traverse, e.g. da Silva and de Oliveira (1998) and Silva et al. (1999), or photogrammetric bridging, in Roncella, Remondino and Forlani (2005). Photogrammetric bridging or traverse is a special BBA (Bundle Block Adjustment) to connect a sequence of stereo pairs and determine the EOP (Exterior Orientation Parameters), as described in Silva, Lemes Neto and Blasechi (2014). In Roncella, Remondino and Forlani (2005), the information from the image sequence is used to bridge the short GPS outages of a mobile mapping system and recover the image orientation parameters. The results of direct georeferencing in challenging urban areas could also be significantly improved by image-based georeferencing with bundle adjustment, as demonstrated by Cavegn, Nebiker and Haala (2016).

Transferring coordinates from areas where GNSS positioning is possible (outdoors) to indoor areas is a challenging task. Strecha, Krull and Betschart (2018) state that data acquisition must be done very carefully to ensure sufficient visual overlap for feature matching and to prevent the models from being separated. There are usually strong illumination changes and large differences in the transition areas (Cohen et al., 2016). The homogeneous and textureless surfaces in indoor environments can lead to a lack of 3D information that can be extracted from the images, according to Cabral and Furukawa (2014). In addition, there are narrow doorways in interior spaces that require complex visibility analysis (Furukawa et al., 2009). Special care should be taken as repetitive patterns in the environment that are recorded in images can lead to errors in image orientation. A small number of point projections, i.e. the number of oriented images in which the point appears, and poor camera angles can lead to outliers. As mentioned in Dierckx, De Veuster and Guidault (2001), with poor camera angles, the angular errors lead to larger position errors. If the GCPs are determined with high accuracy, if they are well distributed and the potential problems mentioned above are avoided, a point cloud or 3D model can be generated for accurate mass positioning of recorded objects.

2 METHODOLOGY

The proposed idea involves a tachymetric survey in combination with photogrammetric methods. Tachymetric measurements were used to determine the exact positions of the GCPs and CPs. The GCPs were used to georeference the photogrammetric traverse, while the CPs were used to quality control the point positions along the traverse. Linked, looped and open photogrammetric traverses were tested. In the open traverse, the GCPs are only set at one end of the traverse. The GCPs are located at both ends of the linked traverse. The looped traverse starts and ends on the same cluster of GCPs.

A total of 42 signalised targets were placed on the test field in the building of the Faculty of Civil and Geodetic Engineering in Ljubljana, Slovenia. 10 of them were outside on the roof of the building (in groups of 5 points in two different parts of the roof), 24 points in two lecture halls and 8 points in corridors and staircases. Five targets on the roof were used as GCPs for the open traverse. Additional four targets in one of the lecture rooms served as GCPs for the linked traverse. Those four targets also served as GCPs for the looped traverse. The rest of the targets were used as CPs. The looped traverse only includes 16 CPs, as it doesn't pass the roof of the building.

2.1 The target

In order to combine tachymetric and photogrammetric measurements, we have designed a target that does justice to both technologies. The design of the target and the target in the test area are shown in Figure 1. It is used both for tachymetric survey – central point for precise positioning - and for photogrammetry as a GCP or CP that can be automatically measured in images. The circle diameter of 38 mm was determined empirically based on the results of the automatic image measurement of the targets with the processing software. The outer dimensions of the target square are 54 x 54 mm. The targets were printed on a retro-reflective film glued to a 2 mm thick kappa plate. The film enabled the use of an electro-optical distance ranging on a total station.

(a) (b)

Figure 1: The target: (a) The design of the target; (b) Target, glued to a wall.

2.2 Tachymetric survey

The coordinates of the targets were determined with an accuracy of better than 3 millimeters. To achieve this accuracy, they were determined in the geodetic network set up in the building. The tachymetric survey was carried out with the Leica Nova MS50 and the precise Leica GPH1P prisms. The measurements were carried out at the points of the geodetic network (prisms) using the automatic target recognition system, while the centers of the targets were sighted manually. The measurements included horizontal directions, zenith distances and slope distances in three repetitions in both faces. The coordinates of all points of the geodetic network were calculated by a 3D adjustment of all measurements based on the precise coordinates of three concrete pillars on the roof of the building. The positions of the pillars were determined with several static GNSS observations. The indirect least squares adjustment, separately for the horizontal coordinates and the heights, was performed with our own program solution in the Matlab environment, according to the procedures in Mikhail and Gracie (1981).

2.3 Image acquisition

The images were taken with the full-frame DSLR camera Nikon D610. We used a fixed 20-mm Nikkor lens with fixed focus and fixed aperture setting during exposure to keep the values of interior orientation constant and minimize the influence of gross observational errors on the estimation of calibration parameters, as recommended by Luhmann, Fraser, and Maas (2016). We used additional illumination in the interior provided by two LED panels with 17000 lumens. The additional light allowed us to close the aperture at least a little to achieve a greater depth of field, as in Mikhail, Bethel, and McGlone (2001). The aperture was set to F/5.6, the ISO value to 640 and the focus to infinity. Exposure times inside the building were mostly between 1/50 and 1/125 second, with only a handful of images taken at 1/30 or 1/40 second. According to the Shutter Speed Photography Guide (2018) and What is the Slowest Shutter Speed (2018), this is at the limit of the slowest shutter speed for handheld photography with the 20 mm lens.

Figure 2: The sequence of images for successful transition through the doors.

Figure 3: Positions and orientations of the images from Figure 2 in the dense cloud.

In the areas of the GCPs, we captured sets of images with multiple scales and convergent images to achieve better accuracy of the final results, according to Micheletti, Chandler, and Lane (2015b). To extend the photogrammetric traverse, an ordered sequence of images with approximately 80% overlap was acquired. Photography of transparent, reflective and homogeneous surfaces was largely avoided. The image sequence followed either a wall or a floor, whereby we mostly photographed the transition between the two, depending on the surface texture. Convergent images were also taken at the corners. We avoided taking divergent images. To minimize the large differences in the sequence of images that could lead to weak key point matching in SfM, special care was taken when moving from one room to another. Several tests proved that the image sequence shown in Figure 2 is the most suitable for passing through the doors. Figure 3 shows the camera positions when passing through the doors.

2.4 Photogrammetric processing

The photogrammetric processing was performed in Agisoft Metashape Pro, which uses SfM to calculate the orientation of the images. Due to the unfavorable conditions for image matching along the traverses, e.g. textureless surfaces, the camera was pre-calibrated (see Section 2.4.1). Calculated parameters of interior orientation were imported in Metashape and used as initial values for self-calibration, performed in SfM.

When processing photogrammetric traverses, the image coordinates of the GCPs were included in the photogrammetric adjustment. Therefore, the deviations of the GCPs and the exterior orientation of all images were calculated and a georeferenced sparse point cloud was generated. The image coordinates of all CPs were also included in the process in order to be able to calculate the coordinate differences in relation to the tachymetric survey. In the final step of photogrammetric processing, a dense point cloud was calculated from the oriented images using MVS.

2.4.1 Camera calibration

The 3D calibration field was set up in one of the lecture halls. Eleven GCPs were marked on the walls. To increase the number of reliable key points for image matching, some posters were placed on the walls and the mirror above the sink was removed. Figure 4 shows the calibration field in the form of a 3D model.

Figure 4: 3D calibration field.

For the camera calibration purposes, 28 convergent and multi-scale images of the test field were captured independently of photogrammetric traverses imaging. The following camera parameters were determined in the process of calibration: f (focal length), cx and cy (principal point coordinates), b1 and b2 (affinity and skew transformation coefficients), k1, k2, k3 and k4 (radial distortion coefficients), p1 and p2 (tangential distortion coefficients). The meaning of the parameters is taken from Agisoft (2018).

3 RESULTS

3.1 Results of the tachymetric survey

We determined the coordinates of all 42 targets of the geodetic network. It consisted of 18 tachymetric stations. We measured 924 triplets of horizontal directions α, zenith distances Z and slope distances d. Depending on the instrument used, the expected precisions were $\overline{\sigma_\alpha} = 1{,}08''$, $\overline{\sigma_Z} = 0{,}92''$ and $\overline{\sigma_d} = 0{,}15$ mm.

The geodetic datum of the geodetic network was determined with the coordinates of the three reference points, which were concrete pillars on the roof of the faculty building. The observations were adjusted as a 3D network according to the principle of least squares. During the adjustment, the actual precisions of the 42 targets were also calculated. The results are presented in Table 1.

Table 1: The precision measures of the coordinates of the targets.

	Min (mm)	Max (mm)	Mean (mm)
σ_e	0,39	1,41	0,75
σ_n	0,52	1,89	0,99
σ_H	0,22	1,09	0,46
σ_{3D}	0,69	2,53	1,33

3.2 Results of the photogrammetric traverses

886 images taken on set formed the basis for the photogrammetric traverses. The courses of the traverses and the target locations are presented in Figure 5 and described in sections 3.2.1 – 3.2.3.

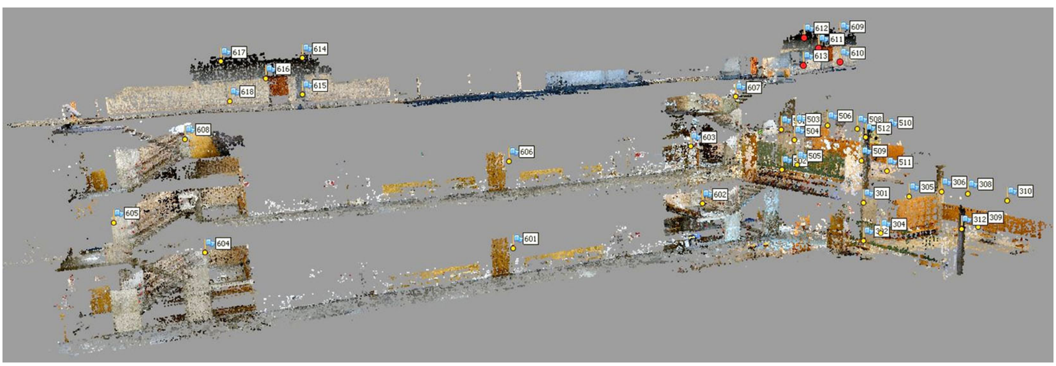

Figure 5: Sparse point cloud with the locations of the targets.

The accuracy of the traverses was assessed by the CPs. We calculated the position errors of the CPs from the coordinate differences of the marker coordinates obtained by the tacheometric survey and the coordinates of the markers obtained during the photogrammetric processing.

3.2.1 Open traverse

The targets 609 – 613 (marked red in Figure 5) on the roof served as GCPs. 3D deviations of the GCPs after the photogrammetric triangulation are between 0.25 and 0.59 mm.

The position errors of the CPs for the open traverse are shown in the 2nd column of Table 2. They are sorted by the value of the position error in ascending order. The distance column refers to the approximate distance from the GCPs, evaluated along the traverse. Number of projections is the number of oriented images on which the position of the target is defined. The last column in Table 2 shows the position errors for the linked traverse, which is described in Section 3.2.2.

Table 2: Check point position errors of the open traverse and for the linked traverse. The distance column refers to the approximate distance from the GCPs of the open traverse.

CP	position error - open (cm)	distance (m)	number of projections	position error - linked (cm)
607	1.42	12	7	0.98
503	1.48	42	78	1.24
506	1.49	42	22	1.29
501	1.56	42	67	1.23
504	1.62	42	75	1.25
508	1.83	44	32	1.53
505	1.90	42	89	1.30
502	2.01	42	2	1.38
603	2.13	32	20	0.87
509	2.13	44	10	1.66
510	2.20	44	22	1.80
511	2.45	44	16	1.97
602	3.25	47	7	0.75
512	3.34	52	8	2.72
301	4.52	74	20	GCP
302	5.11	74	29	0.07
304	5.72	74	28	GCP
305	6.13	74	11	0.10
312	6.90	82	5	0.81
306	7.43	74	4	0.72
614	7.66	37	8	6.07
308	7.79	77	4	GCP
615	8.12	37	26	6.46
309	8.27	77	4	GCP
310	8.77	77	3	0.37
616	8.92	37	24	7.26
617	9.87	37	12	8.17
618	10.09	37	24	8.31
608	11.24	54	4	9.69
606	15.91	49	14	16.30
601	20.35	72	8	19.71
604	58.01	70	6	60.25
605	67.04	78	5	69.90

For the open traverse, the RMSE for all CPs is 17.0 cm. By using the 3*RMSE as a measure for the gross error in position, there are two outliers (604 and 605) with an error of more than 51.0 cm. They occur with a small number of images that have a poor geometric distribution, since the space for the photographing was limited on the stairways. Figure 6 shows a graph of CP errors versus distance without CPs 604 and 605.

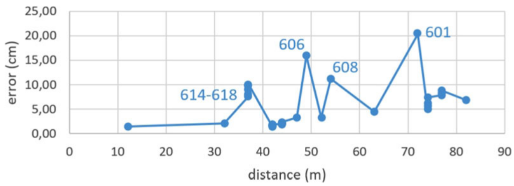

Figure 6: Position error of the CPs in relation to the distance in the open traverse.

According to Figure 6, there are still some CPs with outstanding errors. CPs 614 – 618 are relatively close to the origin (37 meters). CP 608 has a slightly larger error than CPs 614 – 618, as CP 608 is about 15 meters further away from the origin of the traverse. CPs 606 and 601 are set on long walls in corridors and appear on a small number of images with poor geometric distribution.

When CPs 601, 606, 608 and 614-618 are excluded, the graph of position errors changes from that in Figure 6 to that in Figure 7. There are also 3 dotted trend lines: green for linear, red for exponential and orange for 2nd degree polynomial. The exponential and polynomial trend lines fit much better than the linear trend line. From this we can conclude that the position errors could increase uncontrollably with increasing distance from the origin of the traverse.

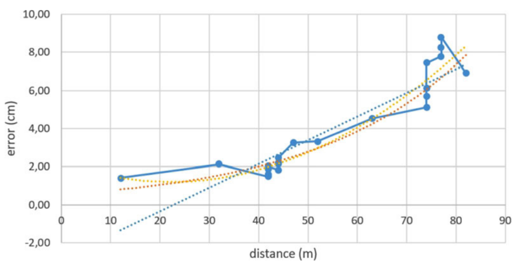

Figure 7: Position error of CPs, gross errors excluded, in relation to distance with trend lines in the open traverse.

3.2.2 Linked traverse

In addition to targets 609 – 613 from the open traverse, targets 301, 304, 308 and 309, which were located in the lower lecture hall, were selected as GCPs for the linked traverse. The position deviations of the GCPs after photogrammetric adjustment are between 0.5 and 1.7 cm.

The position errors of the CPs are listed in the last column of Table 2. CP 512 with the highest position error of 8.6 cm only appeared on 8 images and has poor image geometry as it is located near a window. The second largest position error is less than 2 cm. As expected, the CPs in the lecture hall on the middle level (500+) have the highest errors. A comparison of the position errors of the CPs in the open and the linked traverses is shown in Figure 8. CPs that are more than 5 meters away from the shortest path of the linked traverse (right staircase in Figure 5) were omitted. The distance (in meters) refers to the distance of the CPs from the origin of the open traverse.

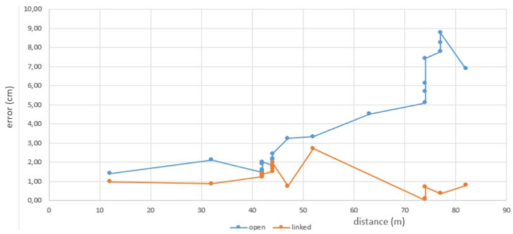

Figure 8: Comparison of CP position errors for open and linked traverses.

3.2.3 Looped traverse

The situation of the selected looped traverse is shown in Figure 9. Although the entire traverse takes place indoors, the same principles can be applied to the outside-inside-outside situation or to the outside-inside coordinate transfer.

The traverse starts in the lower lecture hall (targets 300+), goes through the corridor on the same floor (passes target 601), the opposite staircase (604 and 605), the corridor on the upper floor (606), the upper lecture hall (500+) and the nearby staircase (602, 603) and finally ends in the lower lecture hall.

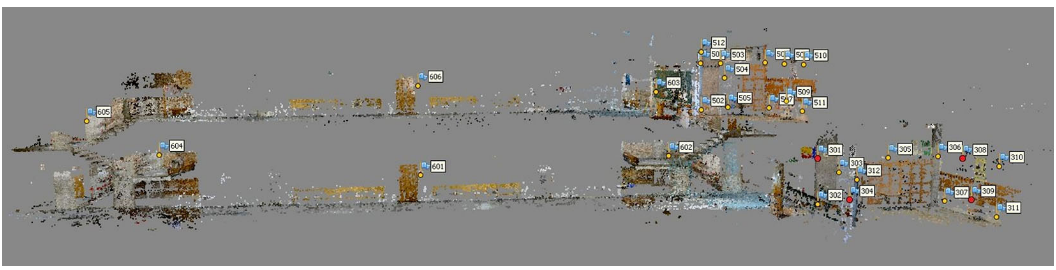

Figure 9: Point cloud and targets in the looped traverse. GCPs are marked in red.

Targets 301, 304, 308 and 309, marked in red in Figure 9, were selected as GCPs for the traverse. The deviations of the GCPs after the photogrammetric adjustment are between 0.34 and 0.62 mm. The position errors of the CPs are listed in Table 3. The table is sorted by ascending values of the position errors.

Table 3: Check point position errors in the looped traverse. The distance column refers to the approximate distance from the origin of the looped traverse.

CP	position error - looped (cm)	distance (m)
303	0.04	0
310	0.08	0
302	0.09	0
306	0.14	0

CP	position error - looped (cm)	distance (m)
312	1.16	11
602	1.37	16
603	1.65	29
601	2.25	27
506	4.12	41
501	4.44	41
509	5.21	41
606	5.62	45
511	6.11	41
604	7.27	54
512	8.57	50
605	11.54	62

It should be noted that CP 605 only appears in four images and that the image geometry is weak because all four projection centers are close to each other. Figure 10 shows a plot of the position errors of the CPs as a function of the distance to the GCPs. Again, there are three trend lines: green for linear, red for exponential and orange for 2nd degree polynomial. The conclusion is similar to the open traverse: Position errors can be significant at larger distances from the reference points.

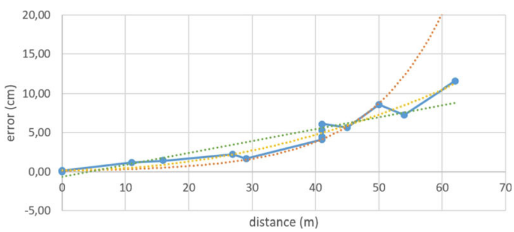

Figure 10: Position errors of check points in relation to distance with trend lines – looped traverse.

3.3. Dense point cloud and mesh, mass positioning

All results in this study are based on the SfM processing that led to the oriented images and the georeferenced sparse point cloud. However, further processing steps can be applied to the data. Using dense image matching algorithm such as MVS can be used to calculate a dense point cloud from oriented images, according to Micheletti, Chandler and Lane (2015b) and Piermattei et al. (2016). Another process can involve the calculation of 3D meshes to create a 3D model from the dense point cloud. A dense point cloud and mesh are by-products of the research and are added here for a visual comparison of the results on a selected section and to illustrate the metric use of the products.

The upper lecture hall with targets 501-512 was selected for the demonstration. The sparse point cloud for the entire area, shown in Figure 5, consists of 653,320 points. The sparse point cloud of a detail in the lecture hall is shown in Figure 11. The dense cloud of the lecture hall alone has 104,389,215 points. The view of the dense point cloud from the same location as in Figure 11 is shown in Figure 12. A 3D mesh was calculated from the dense point cloud. The mesh consists of

20,877,815 faces. Figure 13 shows the textured 3D model from the same point of view as in Figure 11 and Figure 12.

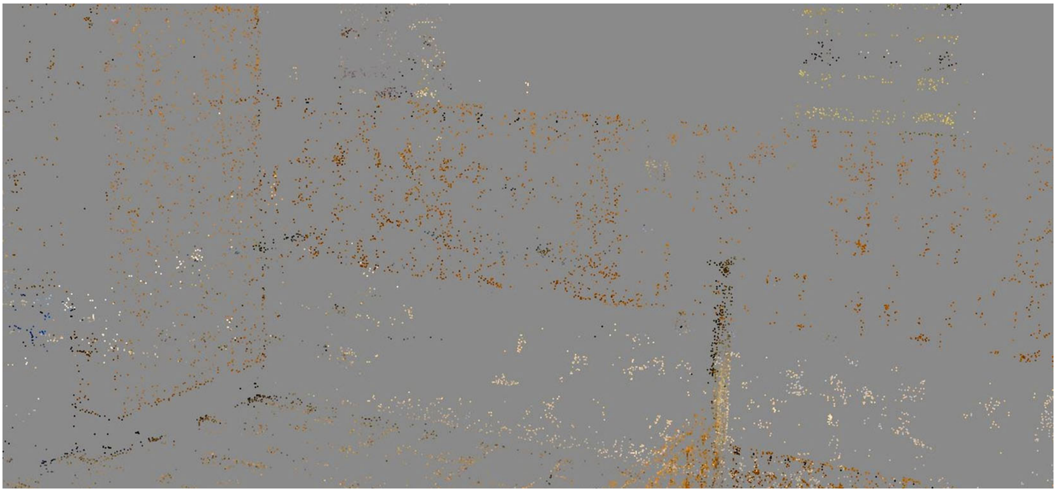

Figure 11: Sparse point cloud.

Figure 12: Dense point cloud.

The dense point cloud is georeferenced, i.e. each of the more than one million points is given a 3D coordinate with easting, northing and elevation. A dense point cloud and a 3D model are therefore suitable for mass positioning. According to the position errors of the CPs in the lecture hall from the open traverse (3.2.1), the accuracy of the positions of the cloud points is about 2 cm (see Table 2).

A 3D model offers the user the possibility to measure the entities of the model, e.g. coordinates or distances, as shown in Figure 14. Figure 14 (a) shows the model coordinates of target 509. The measured coordinates of the target are (460895.4659, 100786.2600, 361.8299). Discrepancies between 7 and 18 mm confirm the accuracy of the model.

Figure 13: Textured 3D mesh representing 3D model

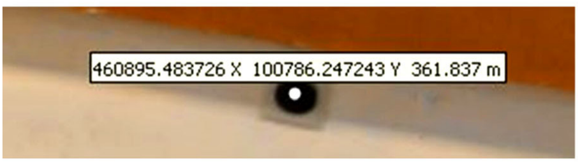

(a)

(b)

Figure 14: Measuring on a 3D model: (a) Coordinates; (b) Distances.

4 DISCUSSION

The position errors on the CPs of the open, linked and looped photogrammetric traverses are presented in section 3. As expected, the accuracy of the open traverse is the lowest, because only the reference coordinates of the origin are known. The position accuracy of the CPs near the origin is in the range of a few cm, but the position error increases with distance from the origin. Special care should be taken with points that appear on a small number of images that have poor image block geometry. On the other hand, a small number of images does not necessarily lead to large errors in CPs, see e.g. target 502 in 3.2.1. It is important that the images are convergent, i.e. taken from different angles, in order to achieve a favorable image ray's geometry.

If the GCPs are only located on one part of the traverse, e.g. at the beginning of the traverse in the open traverse or at the beginning and end of the linked traverse, the number of GCPs is not very significant. In general, 4 to 5 non-collinear distributed GCPs are sufficient. Adding more GCPs at the start or the end of the traverse does not improve the positions of the CPs. On the other hand, as expected, the position accuracy increases when we place additional GCPs at a greater distance from the traverse origin. In general, high accuracy of the GCP coordinates is required to obtain accurate point coordinates in the traverse.

A dense point cloud and a 3D model are very suitable for mass positioning as each point in the cloud contains 3D coordinates. The example presented in Section 3.3 has more than 100 million points and the model does not even cover the entire lecture hall. The accuracy of the positions of the points in the point cloud is similar to that of the nearby CPs.

4.1. Problems with SfM indoors

When processing indoor images with SfM, repetitive patterns can cause problems as the algorithm might match key points in different areas. Some examples can be found in Figure 15. Figure 15 (a) shows a situation in which the fire escape plans caused a misalignment of the images taken on the individual staircases. The result is that only one staircase appears in the point cloud instead of two staircases. In addition, the single staircase contains three sections instead of two, as can be seen in Figure 15 (b) above. The lower part of Figure 15 (b) shows connected lecture halls, which are created by having the same poster on the walls of both halls.

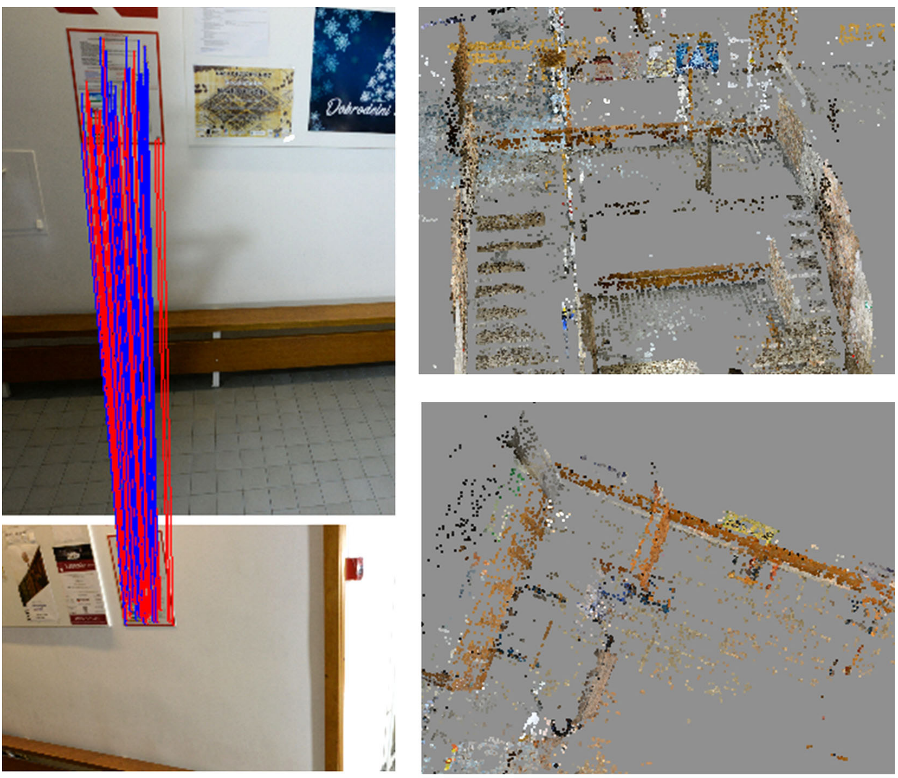

(a) (b)

Figure 15: Problems with repetitive patterns: (a) Aligning wrong images; (b) Faulty models as a result.

Other problematic repetitive patterns are: Emergency exit signs, clocks, fire alarms, etc. The problem can be solved by masking out critical patterns from the images. The process can be iterative because when one pattern is masked out, other problematic patterns may appear.

5 CONCLUSIONS

The proposed solution features a classic surveying traverse, but in a different way than usual, namely with a photo camera instead of a total station. A total station or GNSS is still used to determine the positions of GCPs and CPs, but the rest of the fieldwork and processing is based on photogrammetric principles.

Our tests have shown that the positions of the points along the traverse are still accurate, even when adjusting several hundred images and several dozen meters away from the traverse reference points. A positioning accuracy of 2 cm can even be achieved at a distance of 40 meters from the reference points of the open traverse.

If possible, the use of looped or linked traverses is recommended, as we may count on lower position errors of the points in the point cloud and these provide better quality control. If this is not possible, open traverse can be used, but with caution, as outliers can occur and remain undetected. In general, the repeating patterns can cause misalignment of the image. To avoid such cases, the patterns can be masked out.

The GCPs should be set along horizontal and vertical planes to create a solid basis for the traverse in all three dimensions.

The experiments presented clearly show that the photogrammetric traverse can be used for indoor positioning. The positions of the GCPs outdoors can be determined with tachymetric or GNSS measurements, but no surveying instrument is required for the rest of the path. Since GNSS is not available inside buildings or underground and can only be used to a very limited extent under dense vegetation and in urban canyons, the proposed method is a possible solution in these areas. Moreover, it is not just a point positioning method, but rather a mass positioning method where millions of geo-referenced points can be easily determined.

Mass positioning is not the only product of photogrammetric traverse. A textured 3D model with a high number of faces provides photorealistic scenes, as can be seen in Figure 13. A 3D model enables various visualizations, e.g. views of the model from any perspective and virtual flyovers. It can also be used for various calculations and measurements, e.g. for distances, angles, areas, volumes, etc.

A classical geodetic survey is limited to the measurement of individual points. If the positions of other points in the vicinity of the previously surveyed points need to be determined, the area must be resurveyed. The advantage of photogrammetric traverse is that the survey does not have to be repeated, as the user can reconstruct the 3D position of any point from the oriented images. The disadvantage of photogrammetric traverse is the lack of quality control during data acquisition, as the results are only available after the images have been processed in the office.

In our opinion, photogrammetric traverse might be beneficial not only indoors but also in the natural environment. For photogrammetry itself, there are hardly any repetitive patterns in nature, which means that there are fewer problems with the key point matching that allows the image orientation to be determined. In dense vegetation, GNSS either does not work or is less accurate and tachymetric traverse can be complicated or even impossible. In such an environment, photogrammetric traverse may be the only inexpensive solution. This will be a topic of our further research.

The experiments presented were carried out indoors. Similar conditions can be expected in some challenging outdoor environments, such as urban canyons and dense vegetation. In the latter, both GNSS and tachymetry can be difficult to apply, so photogrammetric traverses could be a very reasonable solution. This is included in the plans for future work.

Funding: The authors acknowledge the financial support from the Slovenian Research Agency (research core funding No. P2-0227 Geoinformation infrastructure and sustainable spatial development of Slovenia and No. P2-0406 Earth Observation and Geoinformatics).

Literature and references:

Agisoft (2018). Agisoft PhotoScan User Manual: Professional Edition, Version 1.4. http://www.agisoft.com/downloads/user-manuals/, accessed on 4. 4. 2018.

Barazzetti, L., Mussio, L., Remondino, F., Scaioni, M. (2012). Targetless Camera Calibration. ISPRS - International Archives of the Photogrammetry, Remote Sensing and Spatial Information Sciences 2012, Vol. XXXVIII-5/W16, 335–342. DOI: 10.5194/isprsarchives-XXXVIII-5-W16-335-2011

Barazzetti, L., Scaioni, M., Remondino, F. (2010). Orientation and 3D modelling from markerless terrestrial images: combining accuracy with automation. The Photogrammetric Record 2010, Vol. 25, No. 132, 356–381. DOI: 10.1111/j.1477-9730.2010.00599.x

Cabral, R., Furukawa, Y. (2014). Piecewise Planar and Compact Floorplan Reconstruction from Images. IEEE Conference on Computer Vision and Pattern Recognition, Columbus, OH, USA, 23-28 June 2014, 628–635. DOI: 10.1109/CVPR.2014.546

Carrivick, J., Smith, M., Quincey, D. (2016). Structure from motion in the geosciences. Wiley-Blackwell: Chichester, UK, Ames, Iowa, USA. DOI:10.1002/9781118895818

Cavegn, S., Nebiker, S., Haala, N. (2016). A Systematic Comparison Of Direct And Image-Based Georeferencing In Challenging Urban Areas. ISPRS - International Archives of the Photogrammetry, Remote Sensing and Spatial Information Sciences 2016, Vol. XLI-B1, 529–536. DOI: 10.5194/isprs-archives-XLI-B1-529-2016

Cohen, A., Schönberger, J.L., Speciale, P., Sattler, T., Frahm, J.M., Pollefeys, M. (2016). Indoor-Outdoor 3D Reconstruction Alignment. In Lecture Notes in Computer Science, vol 9907, Computer Vision – ECCV 2016, Leibe, B., Matas, J., Sebe, N., Welling, M. (Eds.), Springer, 285–300. DOI: 10.1007/978-3-319-46487-9_18

da Silva, J.F.C., de Oliveira, R.A. (1998). Triangulation of a sequence of terrestrial digital images. In ISPRS Archives – Volume XXXII Part 2, Commission II Symposium - Data Integration: Systems and Techniques, Cambridge, UK, 13-17 July 1998, Donoghue, D.N.M., (Ed.), 273–277.

Dierckx, B., De Veuster, C., Guidault, P.A. (2001). Measuring a Geometry by Photogrammetry: Evaluation of the Approach in View of Experimental Modal Analysis on Automotive Structures. Proceedings of the 2001 Noise and Vibration Conference, Traverse City, Michigan, USA, 30 April - 3 May 3 2001.

Elbahnasawy, M. et al. (2018). Multi-Sensor Integration Onboard a UAV-Based Mobile Mapping System for Agricultural Management. IGARSS 2018 - 2018 IEEE International Geoscience and Remote Sensing Symposium, Valencia, Spain, 2018, 3412-3415. DOI: 10.1109/IGARSS.2018.8517370

Furukawa, Y, Curless, B., Seitz, S.M., Szeliski, R. (2009). Reconstructing building interiors from images. IEEE 12th International Conference on Computer Vision, Kyoto, Japan, 29 September - 2 October 2009, 80–87. DOI: 10.1109/ICCV.2009.5459145

Furukawa, Y., Hernández, C. (2015). Multi-View Stereo: A Tutorial. Foundations and Trends in Computer Graphics and Vision: Vol. 9: No. 1-2, 1-148. DOI: 10.1561/0600000052

Luhmann, T., Fraser, C., Maas, H.G. (2016). Sensor modelling and camera calibration for close-range photogrammetry. ISPRS Journal of Photogrammetry and Remote Sensing 2016, Vol. 115, 37–46. DOI: 10.1016/j.isprsjprs.2015.10.006

Micheletti, N., Chandler, J.H., Lane, S.N. (2015a). Investigating the geomorphological potential of freely available and accessible structure-from-motion photogrammetry using a smartphone. Earth Surface Processes and Landforms 2015, Vol. 40, No. 4, 473–486. DOI: 10.1002/esp.3648

Micheletti, N., Chandler, J.H., Lane, S.N. (2015b). Structure from motion (SFM) photogrammetry. In Geomorphological Techniques (Online Edition), Clarke, L.E., Nield, J.M. (Eds.). British Society for Geomorphology: London, UK. https://hdl.handle.net/2134/17493

Mikhail, E.M., Bethel, J.S., McGlone, J.C. (2001). Introduction to modern photogrammetry. John Wiley, New York, USA.

Mikhail, E.M., Gracie, G. (1981). Analysis And Adjustment Of Survey Measurements, Van Nostrand Reinhold, New York.

Nadal-Romero, E., Revuelto, J., Errea, P., López-Moreno, J. I. (2015). The application of terrestrial laser scanner and SfM photogrammetry in measuring erosion and deposition processes in two opposite slopes in a humid badlands area (central Spanish Pyrenees). SOIL, 1, 561–573. DOI:10.5194/soil-1-561-2015

Piermattei, L., Carturan, L., De Blasi, F., Tarolli, P., Dalla Fontana, G., Vettore, A., Pfeifer, N. (2016). Suitability of ground-based SfM–MVS for monitoring glacial and periglacial processes. Earth Surf. Dyn. 2016, 4, 425–443. DOI: 10.5194/esurf-4-425-2016

Remondino, F., Spera, M.G., Nocerino, E., Menna, F., Nex, F. (2014). State of the art in high density image matching. The Photogrammetric Record 2014, Vol. 29, No. 146, pp. 144–166. DOI 10.1111/phor.12063

Roncella, R., Remondino, F., Forlani, G. (2005). Photogrammetric bridging of GPS outages in mobile mapping. In Proceedings Volume 5665, Videometrics VIII, Proceedings of the Electronic Imaging 2005, San Jose, USA, p. 308. DOI: 10.1117/12.587843

Rupnik, E., Daakir, M., Pierrot Deseilligny, M. (2017). MicMac – a free, open-source solution for photogrammetry. Open Geospatial Data, Software and Standards 2017, Vol. 2, No. 1. DOI: 10.1186/s40965-017-0027-2

Shutter Speed Photography Guide (2018). https://www.davemorrowphotography.com/shutter-speed-chart, accessed on 17. 12. 2018.

Silva, A.R., Batista, J.C., Oliveira, R.A., Camargo, P.O., Silva, J.F.C. (1999). Surveying and mapping of urban streets by photogrammetric traverse. In Proceedings International Workshop on Mobile Mapping Technology, Bangkok, Thailand, 21-23 April 1999, 192–195.

Silva, J.F.C., Lemes Neto, M.C., Blasechi, V. (2014). Automating the Photogrammetric Bridging Based on MMS Image Sequence Processing. ISPRS - International Archives of the Photogrammetry, Remote Sensing and Spatial Information Sciences 2014, Vol. XL–1, 389–396. DOI: 10.5194/isprsarchives-XL-1-389-2014

Strecha, C., Krull, M., Betschart, S. (2018). The Chillon Project: Aerial/Terrestrial and indoor integration. http://www.ee.co.za/wp-content/uploads/2014/11/positionit-nov-dec2014-p4647485051.pdf, accessed 24. 12. 2018.

Wang, G.Q. (2013). Millimeter-accuracy GPS landslide monitoring using Precise Point Positioning with Single Receiver Phase Ambiguity (PPP-SRPA) resolution: a case study in Puerto Rico. Journal of Geodetic Science 2013, Vol. 3, No. 1, 22-31. DOI: 10.2478/jogs-2013-0001

Westoby, M.J., Brasington, J., Glasser, N.F., Hambrey, M.J., Reynolds, J.M. (2012). 'Structure-from-Motion' photogrammetry: A low-cost, effective tool for geoscience applications. Geomorphology 2012, Vol. 179, 300–314. DOI: 10.1016/j.geomorph.2012.08.021

What is the Slowest Shutter Speed You Can Use for Handheld Photography? (2018). https://www.picturecorrect.com/tips/what-is-the-slowest-shutter-speed-you-can-use-for-handheld-photography, accessed on 17. 12. 2018.

Fotogrametrični poligon za zajem podatkov v zaprtih prostorih

OSNOVNE INFORMACIJE O ČLANKU

GLEJ STRAN 148

1 UVOD

Glavni namen raziskave je inovativen način masovnega zajema podatkov, ki združuje postopke klasičnega geodetskega poligona in fotogrametrije. Najbolj običajni geodetski merski metodi sta tahimetrija in GNSS (angl. *global navigation satellite systems*). Obe omogočata visoko natančnost določitve položaja, do nivoja mm, kot navaja Wang (2013), vendar pa za obe metodi velja, da se določa položaj zgolj ene točke naenkrat. Masovni zajem prostorskih podatkov vzdolž poligona je mogoč tudi s terestričnim laserskim skeniranjem (TLS) ali mobilnimi merilnimi sistemi (MMS). Fotogrametrični poligon je tu predstavljen kot alternativa prenosnemu MMS, ki ga držimo v roki ali je nameščen na vozičku. Tak sistem je veliko dražji kot fotoaparat. Fotogrametrični poligon se na terenu izvede hitreje kot izmera s TLS (Nadal-Romero et al., 2015). Fotogrametrična obdelava pa zahteva nekaj več dela v pisarni.

S poligonom razširimo mrežo obstoječih referenčnih točk na območja, kjer ni referenčnih točk. S tahimetrično izmero lahko razvijemo poligon od ene do druge skupine danih točk (priklepni poligon), začnemo in končamo na isti skupini danih točk (zaključeni poligon) ali ga zaključimo na novih točkah (slepi poligon). Priklepni in zaključeni poligon omogočata doseganje visoke natančnosti določanja položaja točk, medtem ko pri slepem poligonu ni nadzora kakovosti.

V članku predstavljamo vse tri vrste poligonov (priklepni, zaključeni in slepi), razvite iz fotografij, ki se medsebojno prekrivajo. Fotografije smo obdelali z metodo grajenja strukture iz gibanja (angl. SfM – *structure from motion*). SfM uporablja množico fotografij z visoko stopnjo prekrivanja in algoritme slikovnega ujemanja za hkratno določitev parametrov notranje in zunanje orientacije fotografij ter 3D rekonstrukcijo površja v obliki redkega oblaka točk (Rupnik, Daakir in Pierrot Deseilligny, 2017; Carrivick, Smith in Quincey, 2016; Westoby et al., 2012, ter Barazzetti, Scaioni in Remondino, 2010). V kritičnem pregledu algoritmov za gosto slikovno ujemanje (Remondino et al., 2014) so orodja SfM razvrščena v tako imenovano kategorijo »black-box«, kjer lahko pride do divergence v fotogrametrični triangulaciji ali do geometrijskih deformacij. Zato je treba v izravnavo bloka fotografij obvezno vključiti objektne in slikovne koordinate oslonilnih točk (OT). OT so natančno izmerjene v objektnem koordinatnem sistemu in so običajno signalizirane s tarčami, kar omogoča samodejno določitev njihovih slikovnih koordinat. Posebno pozornost je treba nameniti samokalibraciji fotoaparata, ki je vključena v SfM. Barazzetti et al. (2012) ter Micheletti, Chandler in Lane (2015a) trdijo, da naj bi bil fotogrametrični blok sestavljen iz konvergentnih in zasukanih fotografij v različnih merilih, kar ojača geometrijo bloka za izračun notranje orientacije v postopku samokalibracije. Zadostna razlika v merilu fotografij omogoča zanesljivo določitev parametrov notranje orientacije fotoaparata (Luhmann Fraser in Maas, 2016).

Za pridobitev zanesljivih metričnih informacij in oceno točnosti rezultatov smo vzpostavili mrežo signaliziranih OT na začetku, vzdolž in na koncu poligona. OT smo uporabili za georeferenciranje oblaka točk, izdelanega iz fotografij. Točnost metod smo ocenili glede na koordinatne razlike na več kontrolnih točkah (KT), ki so bile izmerjene vzdolž poligona. Za določitev položaja OT in KT običajno uporabimo metode izmere, kot so tahimetrija ali GNSS. V nasprotju s točkovno določitvijo položaja s tahimetrijo ali GNSS fotogrametrični poligon zagotavlja masovni zajem več milijonov točk na območjih, kjer se iz orientiranih fotografij izračuna gost oblak točk. Gosti oblak točk izračunamo z algoritmi za gosto slikovno ujemanje, običajno je to večpogledni stereo (angl. MVS – *multi-view stereo*), ki sta ga razvila Furukawa in Hernández (2015).

Podobne metode, bodisi iz terestričnih fotografij (Silva, Lemes Neto in Blasechi, 2014; Roncella, Remondino in Forlani, 2005) ali fotografij z letalnika (Elbahnasawy et al., 2018), so razširjene pri obdelavi podatkov MMS na območjih, kjer je prišlo do izpada signala GNSS. Avtorji tovrstne metode pogosto imenujejo fotogrametrični poligon (angl. *photogrammetric traverse*), na primer da Silva in de Oliveira (1998) ter Silva et al. (1999), oziroma fotogrametrično premoščanje (angl. *photogrammetric bridging*), kot navajajo Roncella, Remondino in Forlani (2005). Fotogrametrični poligon oziroma fotogrametrično premoščanje je poseben primer fotogrametrične triangulacije, s katero povežemo zaporedje stereoparov in določimo parametre zunanje orientacije fotografij (Silva, Lemes Neto in Blasechi, 2014). Roncella, Remondino in Forlani (2005) so prav tako zapisali, da se informacija z zaporedja fotografij uporabi za premoščanje kratkih izpadov signala GNNS na sistemih MMS in za izračun orientacije fotografij. Rezultati direktnega georeferenciranja v oteženih urbanih okoljih se lahko občutno izboljšajo s podporo orientacijskih parametrov, ki jih pridobimo z izravnavo fotogrametričnega bloka (Cavegn, Nebiker in Haala, 2016).

Prenos koordinat z območij, kjer je izmera GNSS mogoča, torej na odprtem, v notranjost objektov je zahtevna naloga. Strecha, Krull in Betschart (2018) trdijo, da mora biti fotografiranje izvedeno previdno, da se zagotovi zadosten preklop med fotografijami za slikovno ujemanje in pridobitev enotnega modela površja. Na prehodnih območjih so po navadi velike razlike v osvetljenosti, kot ugotavlja Cohen et al. (2016). Homogene ploskve brez tekstur v notranjosti objektov otežujejo pridobivanje 3D podatkov iz fotografij (Cabral in Furukawa, 2014). Dodatna ovira so ozki prehodi skozi vrata, ki zahtevajo kompleksno analizo vidnosti, kot pišejo Furukawa et al. (2009). Posebno pozornost je treba nameniti vzorcem, ki se ponavljajo na različnih fotografijah in lahko vodijo do napačnih orientacij fotografij. Nizko število projekcij točk, to je število orientiranih fotografij, kjer se točka pojavi, lahko povzroči pojav grobih pogreškov. Dierckx, De Veuster in Guidault (2001) omenjajo, da lahko slaba geometrična razporeditev fotografij vodi do velikih položajnih pogreškov. Če so OT določene z visoko stopnjo točnosti in če so dobro razporejene ter hkrati preprečimo pojav zgoraj navedenih težav, lahko pridobimo točen oblak točk ali 3D model za pozicioniranje velikega števila točk zajetega objekta oziroma območja.

2 METODOLOGIJA

Predlagana metoda vključuje tahimetrično izmero v kombinaciji s fotogrametričnimi metodami. Tahimetrične meritve smo uporabili za točno določitev položajev OT in KT. OT so služile za georeferenciranje fotogrametričnega poligona, medtem ko smo s KT ocenili kakovost položaja točk vzdolž poligona. Preizkusili smo priklepni, zaključeni in slepi poligon. Pri slednjem so OT zgolj na enem koncu poligona, pri priklepnem poligonu OT na obeh krajiščih poligona, zaključen poligon se začne in konča na isti gruči OT.

V stavbi Fakultete za gradbeništvo in geodezijo Univerze v Ljubljani smo signalizirali 42 točk. Deset točk je bilo zunaj, na strehi stavbe, 24 točk v dveh predavalnicah in 8 točk na hodnikih in stopniščih. Pet točk na strehi smo uporabili kot OT pri slepem poligonu. Dodatne štiri točke v eni od predavalnic smo uporabili kot OT za priklepni poligon. Te štiri točke so imele vlogo OT za zaključeni poligon. Ostale točke smo uporabili kot KT. Zaključeni poligon vključuje le 16 KT, saj ga nismo razvili na streho stavbe.

2.1 Tarča

Za namen združitve tahimetrične in fotogrametrične izmere smo izdelali tarčo, ki je zadoščala obema tehnologijama. Zasnova tarče in primer njene stabilizacije sta prikazani na sliki 1. Tarča je uporabna za tahimetrično izmero – središčna točka za natančno viziranje – in kot fotogrametrična OT ali KT, ki omogoča samodejno merjenje slikovnih koordinat. Premer kroga 38 mm je bil določen empirično na podlagi rezultatov samodejnih meritev tarč v uporabljeni programski opremi. Zunanje mere tarče so 54 x 54 mm. Tarče so natisnjene na retro-odbojno folijo, nalepljeno na 2 mm debelo tako imenovano kapo ploščo. Folija je omogočila uporabo elektro-optičnega razdaljemera na tahimetru.

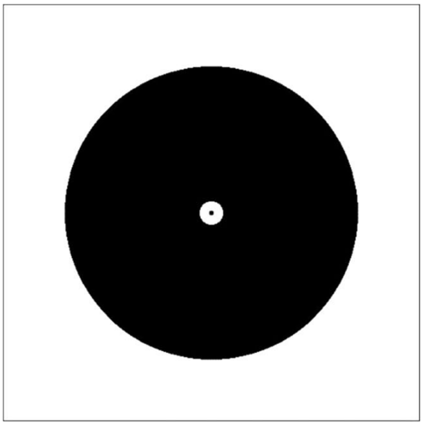

(a)

(b)

Slika 1: Tarča: (a) zasnova tarče; (b) tarča, prilepljena na steni.

2.2 Tahimetrična izmera

Položaje tarč smo določili s točnostjo, boljšo od 3 mm. Za dosego te točnosti smo v stavbi vzpostavili geodetsko mrežo. Tahimetrična izmera je bila izvedena s tahimetrom Leica Nova MS50 in natančnimi prizmami Leica GPH1P. Grobo viziranje tarč je bilo samodejno, natačno viziranje centra tarče smo opravili ročno. V treh ponovitvah v obeh krožnih legah smo izmerili horizontalne smeri, zenitne razdalje in poševne razdalje. Koordinate vseh točk geodetske mreže smo izračunali s 3D izravnavo. Za koordinatno osnovo smo vzeli koordinate betonskih stebrov na strehi stavbe, ki so bile večkrat določene s statičnimi opazovanji GNSS. Za izravnavo smo uporabili posredno metodo najmanjših kvadratov, ločeno za horizontalne koordinate in višine, po postopkih, opisanih v Mikhail in Gracie (1981).

2.3 Fotografiranje

Za fotografiranje smo uporabili polnoformatni DSLR fotoaparat Nikon D610. Uporabili smo fiksni objektiv Nikkor z goriščno razdaljo 20 mm. Kot priporočajo Luhmann, Fraser in Maas (2016), smo pri fotografiranju uporabili konstantno razdaljo fokusiranja in konstantno odprtino zaslonke, s čimer smo zagotovili konstantne parametre notranje orientacije in tako minimizirali možnost pojava grobih pogreškov v postopku kalibracije fotoaparata. V notranjosti smo za dodatno osvetlitev poskrbeli z dvema LED-paneloma s svetilnostjo 17000 lumnov. Boljša osvetlitev je omogočila uporabo manjše odprtine zaslonke, s čimer povečamo globinsko ostrino (Mikhail, Bethel in McGlone, 2001). Odprtino zaslonke smo nastavili na F/5,6, občutljivost senzorja na vrednost ISO 640 in razdaljo fokusiranja na neskončnost. Časi ekspozicije v notranjosti stavbe so bili večinoma med 1/50 in 1/125 sekunde, le nekaj fotografij je imelo daljši čas osvetlitve, 1/30 oziroma 1/40 sekunde. Glede na priporočila v Shutter Speed Photography Guide (2018) in What is the Slowest Shutter Speed (2018) so to robni časi odprtosti zaklopa za fotografiranje iz roke z 20 mm objektivom.

Slika 2: Zaporedje fotografij ob uspešnem prehodu skozi vrata.

Slika 3: Položaji in usmerjenost fotografij, predstavljenih na sliki 2, v gostem oblaku točk.

Na območjih z OT smo posneli več konvergentnih fotografij z različnimi merili za dosego boljše točnosti končnih rezultatov, kot so ugotovili tudi Micheletti, Chandler in Lane (2015b). Za razvijanje fotogrametričnega poligona smo fotografirali s približno 80-odstotnim prekrivanjem. Izogibali smo se fotografiranja prosojnih, zrcalnih in homogenih površin. Zaporedje fotografij je sledilo tlom ali steni, največkrat pa smo fotografirali ravno prehod med njima. Na vogalih smo posneli dodatne konvergentne fotografije. Izogibali smo se divergentnim fotografijam. Za zmanjšanje velikih razlik med zaporednimi fotografijami, ki bi lahko povzročile slabo slikovno ujemanje, smo posebno pozornost namenili prehodom iz enega prostora v drugega. Na podlagi predhodno izvedenih testov smo kot najbolj primeren način prehoda skozi vrata izbrali način, ki je prikazan na sliki 2. Slika 3 prikazuje položaje in usmerjenost fotografij v prehodu.

2.4 Fotogrametrična obdelava

Fotografije smo obdelali v programu Agisoft Metashape Pro, ki za izračun orientacije fotografij uporablja SfM. Zaradi neugodnih pogojev za slikovno ujemanje vzdolž poligona, kjer je bilo kar nekaj monotonih površin brez teksture, smo fotoaparat predkalibrirali (glej 2.4.1). Izračunane parametre notranje orientacije smo uvozili v Metashape in jih uporabili kot začetne vrednosti za samokalibracijo v SfM.

V izravnavo fotogrametričnega poligona smo vključili slikovne koordinate OT in tako pridobili odstopanja na OT ter georeferenciran redek oblak točk. Slikovne koordinate KT so bile prav tako vključene v izravnavo, na njih smo izračunali koordinatna odstopanja glede na tahimetrično izmero. V zaključnem koraku fotogrametrične obdelave je program iz orientiranih fotografij z MVS izračunal še gosti oblak točk.

2.4.1 Kalibracija fotoaparata

3D kalibracijsko polje smo vzpostavili v eni od predavalnic, ki je imela na stenah signaliziranih enajst OT. Za povečanje števila zanesljivih veznih točk v postopku slikovnega ujemanja smo na stene namestili nekaj plakatov in odstranili ogledalo nad umivalnikom. Slika 4 prikazuje kalibracijsko polje, predstavljeno s 3D modelom.

Slika 4: Kalibracijsko polje.

Za kalibracijo fotoaparata smo posneli 28 konvergentnih fotografij v različnih merilih. Fotografiranje za kalibracijo fotoaparata smo izvedli ločeno od fotografiranja poligonov. V postopku kalibracije smo izračunali naslednje parametre notranje orientacije: f (goriščna razdalja), cx in cy (koordinate glavne točke), b1 in b2 (afiniteta in strig), k1, k2, k3 in k4 (koeficienti radialne distorzije) ter p1 in p2 (koeficienta tangencialne distorzije). Podane oznake parametrov notranje orientacije so privzete iz Agisoft (2018).

3 REZULTATI

3.1 Rezultati tahimetrične izmere

Vseh 42 točk geodetske mreže smo določili s tahimetrično izmero z 18 stojišč. Izmerili smo 924 trojic horizontalnih smeri α, zenitnih razdalj Z in poševnih razdalj d. Glede na uporabljen instrument so bile pričakovane natančnosti meritev $\overline{\sigma_\alpha} = 1{,}08''$, $\overline{\sigma_Z} = 0{,}92''$ in $\overline{\sigma_d} = 0{,}15$ mm.

Geodetski datum je bil določen s koordinatami referenčnih točk na treh betonskih stebrih na strehi stavbe. Opazovanja smo izravnali po metodi najmanjših kvadratov. V postopku izravnave smo izračunali natančnosti določitve položajev vseh 42 tarč. Rezultati so predstavljeni v preglednici 1.

Preglednica 1: Natančnosti koordinat tarč

	Min. (mm)	Maks. (mm)	Sred. vredn. (mm)
σ_e	0,39	1,41	0,75
σ_n	0,52	1,89	0,99
σ_H	0,22	1,09	0,46
σ_{3D}	0,69	2,53	1,33

3.2 Rezultati fotogrametričnih poligonov

Fotogrametrične poligone smo razvili iz 886 fotografij, ki smo jih posneli na delovišču. Poteki poligonov in položaji tarč so prikazani na sliki 5 in opisani v poglavjih 3.2.1–3.2.3.

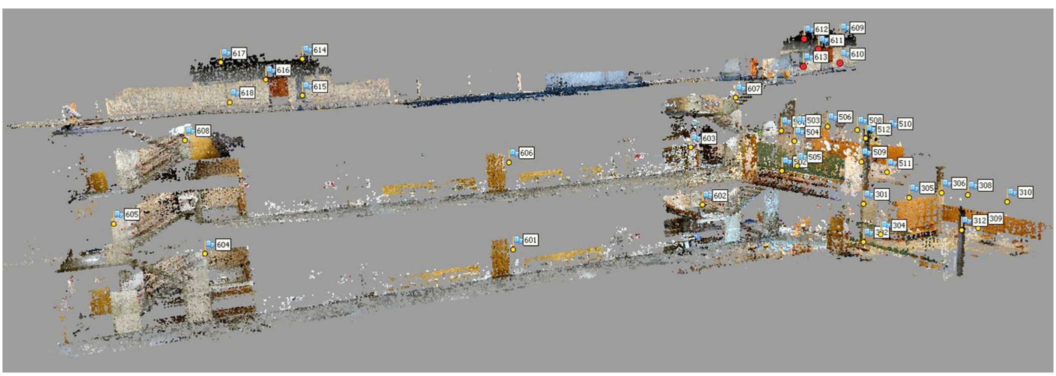

Slika 5: Redek oblak točk s položaji tarč.

Točnost poligonov smo ocenili s KT. Položajna odstopanja na KT smo izračunali kot razliko koordinat tarč, pridobljenih s tahimetrično izmero, in koordinat tarč, izračunanih v fotogrametrični obdelavi.

3.2.1 Slepi poligon

Tarče 609–613 (označene rdeče na sliki 5) na strehi so služile kot OT. Odstopanja na teh točkah po fotogrametrični triangulaciji so bila med 0,25 in 0,59 mm.

Odstopanja v 3D položaju KT slepega poligona so zapisana v drugem stolpcu preglednice 2. Razvrščena so v naraščajočem vrstnem redu glede na odstopanja. Vrednosti v tretjem stolpcu predstavljajo približno razdaljo od OT, merjeno vzdolž poligona. Število projekcij pomeni število orientiranih fotografij, na katerih smo izmerili položaj tarče. Zadnji stolpec v preglednici 2 predstavlja 3D položajna odstopanja za priklepni poligon, ki je opisan v 3.2.2.

Preglednica 2: Položajna odstopanja na KT za slepi in priklepni poligon. Stolpec razdalja podaja približne razdalje od oslonilnih točk slepega poligona.

KT	Polož. odstop. – slepi (cm)	Razdalja (m)	Število projekcij	Polož. odstop. – prikl. (cm)
607	1,42	12	7	0,98
503	1,48	42	78	1,24
506	1,49	42	22	1,29
501	1,56	42	67	1,23
504	1,62	42	75	1,25
508	1,83	44	32	1,53
505	1,90	42	89	1,30
502	2,01	42	2	1,38
603	2,13	32	20	0,87
509	2,13	44	10	1,66
510	2,20	44	22	1,80
511	2,45	44	16	1,97
602	3,25	47	7	0,75
512	3,34	52	8	2,72
301	4,52	74	20	OT
302	5,11	74	29	0,07
304	5,72	74	28	OT
305	6,13	74	11	0,10
312	6,90	82	5	0,81
306	7,43	74	4	0,72
614	7,66	37	8	6,07
308	7,79	77	4	OT
615	8,12	37	26	6,46
309	8,27	77	4	OT
310	8,77	77	3	0,37
616	8,92	37	24	7,26
617	9,87	37	12	8,17
618	10,09	37	24	8,31
608	11,24	54	4	9,69
606	15,91	49	14	16,30
601	20,35	72	8	19,71
604	58,01	70	6	60,25
605	67,04	78	5	69,90

Za slepi poligon je koren srednjega kvadratnega pogreška (angl. RMSE) za vse KT znašal 17,0 cm. Če uporabimo prag za odkrivanje grobih pogreškov 3*RMSE, odkrijemo dva groba pogreška, na točkah 604 in 605, kjer je razlika večja od 51 cm. Ti točki se pojavita na malo fotografijah, ki niso optimalno razporejene, ker je bil prostor za fotografiranje na stopnišču omejen. Slika 6 prikazuje primerjavo razlik na KT glede na razdaljo od OT, brez upoštevanih točk 604 in 605.

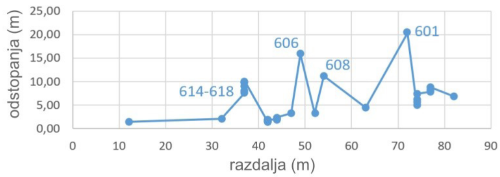

Slika 6: Položajna odstopanja na KT glede na razdaljo v slepem poligonu.

Glede na sliko 6 se na nekaterih KT še vedno pojavljajo večja odstopanja. Točke 614–618 so relativno blizu začetka poligona (37 metrov). Točka 608 ima malenkost večjo odstopanje na KT kot gruča 614–618, je pa ta točka približno 15 m dlje od izhodišča. Točki 606 in 601 sta na dolgih hodnikih in se pojavita na malo fotografijah, ki so slabo prostorsko razporejene.

Če odstranimo točke 601, 606, 608 in 614–618, dobimo prikaz položajnih razlik, kot ga vidimo na sliki 7. Na sliko 7 so dodane tri regresijske krivulje: zelena za linearni, rdeča za eksponentni in oranžna za polinom druge stopnje. Videti je, da se eksponentna in polinomska črta bolje prilagajata točkam kot linearna črta. Iz tega lahko sklepamo, da položajna odstopanja v slepem poligonu naraščajo preko vseh meja z oddaljenostjo od izhodišča poligona.

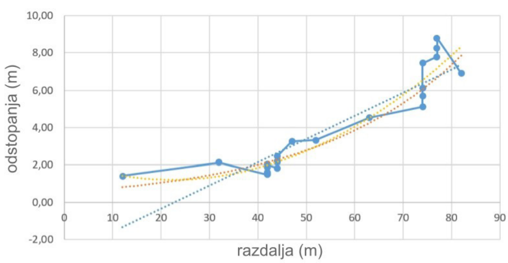

Slika 7: Položajna odstopanja na KT, brez grobih pogreškov, glede na dolžino slepega poligona.

3.2.2 Priklepni poligon

Poleg točk 609–613, ki so imele vlogo OT v slepem poligonu, smo za priklepni poligon dodatno vključili OT 301, 304, 308 in 309, ki se nahajajo v spodnji predavalnici. Odstopanja na oslonilnih točkah po fotogrametrični triangulaciji so med 0,5 in 1,7 cm.

Odstopanja v 3D položaju KT so zapisana v zadnjem stolpcu preglednice 2. Točka 512 z največjim odstopanjem 8,6 cm se nahaja v bližini okna in je bila zajeta na osmih fotografijah, ki so slabo prostorsko razporejene. Drugo največje odstopanje je manjše od 2 cm. Po pričakovanjih so največja odstopanja v predavalnici na srednjem nivoju (oznake 500+). Primerjava položajnih odstopanj na KT slepega in priklepnega poligona je prikazana na Sliki 8. KT, ki so oddaljene več kot 5 metrov od najkrajše linije priklepnega poligona (desno stopnišče na sliki 5), so izločene iz prikaza. Razdalja predstavlja približno oddaljenost KT od začetka poligona.

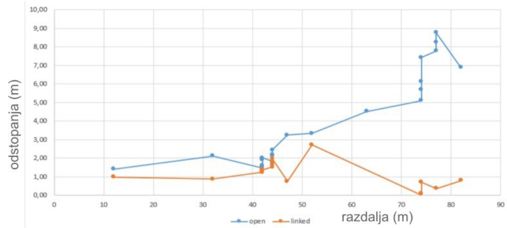

Slika 8: Primerjava odstopanj na KT za slepi in priklepni poligon.

3.2.3 Zaključeni poligon

Situacija zaključenega poligona je prikazana na sliki 9. Četudi je celoten poligon v notranjosti stavbe, se lahko isti postopek uporabi v situaciji zunaj-notri-zunaj ali za prenos koordinat iz zunanjosti v notranjost.

Poligon se prične v spodnji predavalnici (točke 300+), se razvija po hodniku v isti etaži (mimo 601), stopnišču (604 in 605), hodniku v zgornjem nadstropju (mimo 606), v zgornjo predavalnico (500+), po stopnišču (602 in 603) nazaj v začetno predavalnico.

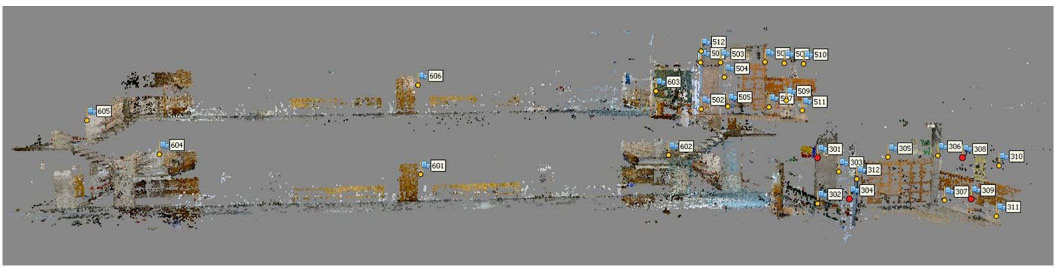

Slika 9: Oblak točk in tarče v zaključenem poligonu. OT so obarvane rdeče.

Točke 301, 304, 308 in 309 so bile izbrane kot OT za zaključeni poligon. Odstopanja na teh točkah po fotogrametrični triangulaciji so med 0,34 in 0,62 mm. Položajna odstopanja na KT so zapisana v preglednici 3. Vrednosti so razvrščene naraščajoče glede na odstopanja.

Preglednica 3: Položajna odstopanja na KT v zaključenem poligonu. Razdalja predstavlja približno oddaljenost od izhodišča poligona.

KT	Polož. odstop. – zaključ. (cm)	Razdalja (m)
303	0,04	0
310	0,08	0
302	0,09	0
306	0,14	0
312	1,16	11

KT	Polož. odstop. – zaključ. (cm)	Razdalja (m)
602	1,37	16
603	1,65	29
601	2,25	27
506	4,12	41
501	4,44	41
509	5,21	41
606	5,62	45
511	6,11	41
604	7,27	54
512	8,57	50
605	11,54	62

Treba je omeniti, da se točka 605 nahaja na zgolj štirih slabo razporejenih fotografijah, saj so vsi štirje projekcijski centri zelo skupaj. Slika 10 prikazuje položajna odstopanja na KT glede na razdaljo od začetka poligona. Ponovno so prikazane tri regresijske krivulje: zelena za linearni, rdeča za eksponentni in oranžna za polinom druge stopnje. Sklep je podoben kot pri slepem poligonu. Položajna odstopanja se povečujejo z oddaljenostjo od referenčnih točk.

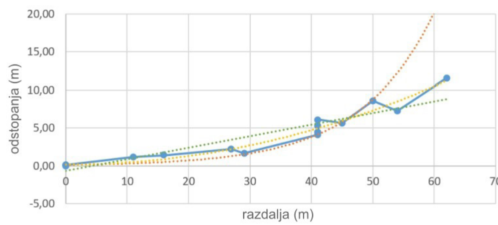

Slika 10: Položajna odstopanja na KT in regresijske krivulje – zaključeni poligon.

3.3 Gost oblak točk in 3D model, določanje položaja večje množice točk

Vsi rezultati v tej raziskavi temeljijo na postopku SfM, katerega rezultat so orientirane fotografije in georeferenciran redek oblak točk. Temu lahko sledijo nadaljnji koraki. Z uporabo algoritmov gostega slikovnega ujemanja, kot je MVS, lahko izdelamo gost oblak točk, kot navajajo Micheletti, Chandler in Lane (2015b) ter Piermattei et al. (2016). Dodatno lahko iz gostega oblaka točk izračunamo poligonsko 3D mrežo, ki predstavlja 3D model površja. Gost oblak točk in 3D model sta stranska izdelka raziskave in sta tu dodana za vizualno primerjavo rezultatov na izbranem območju in za prikaz metrične uporabe izdelkov.

Predstavljamo rezultate za zgornjo predavalnico, v kateri so točke 501–512. Redek oblak točk celotnega območja, prikazan na sliki 5, vsebuje 653.320 točk. Redek oblak točk izbranega detajla v predavalnici je prikazan na sliki 11. Gost oblak točk zgolj predavalnice ima 104.389.215 točk. Identičen pogled na gost oblak točk kot na redek oblak točk s slike 11 prikazuje slika 12. 3D model, izdelan iz gostega oblaka točk, vsebuje 20.877.815 ploskev. Slika 13 prikazuje teksturiran 3D model z istim pogledom kot na slikah 11 in 12.

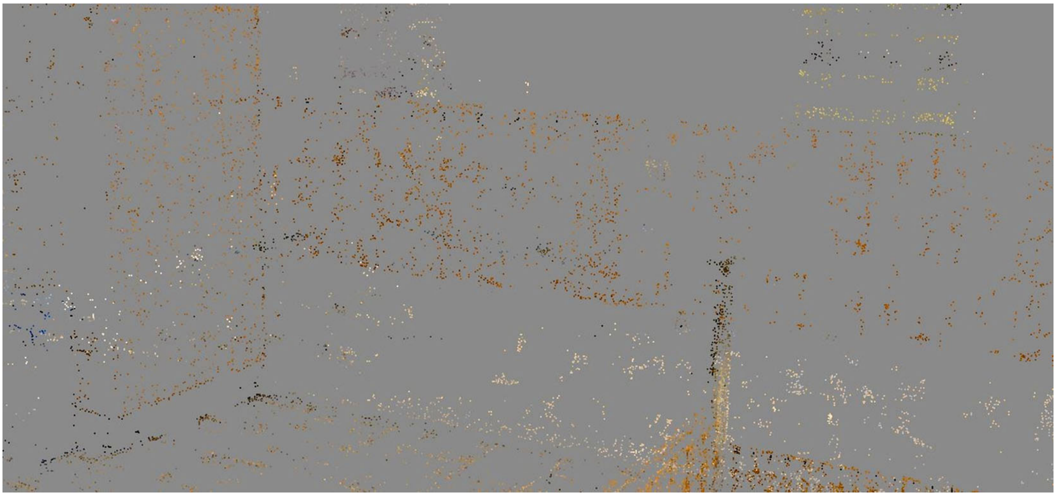

Slika 11: Redek oblak točk.

Slika 12: Gost oblak točk.

Gost oblak točk je georeferenciran, kar pomeni, da ima vsaka točka v oblaku 3D koordinato s horizontalnim položajem in višino. Gost oblak točk in 3D model sta torej primerna za določanje položajev večjega števila točk. Glede na položajna odstopanja na KT v predavalnici, izračunane v slepem poligonu (3.2.1), je točnost položajev v oblaku točk okoli 2 cm (glej preglednico 2).

3D model ponuja možnost merjenja v samem modelu, na primer koordinate ali razdalje, kot je prikazano na sliki 14. Slika 14 (a) prikazuje modelne koordinate tarče 509. Izmerjene koordinate te točke so (460895,4659 m, 100786,2600 m, 361,8299 m). Odstopanja med 7 in 18 mm potrjujejo metrično točnost modela.

Slika 13: Teksturiran 3D model.

(a)

(b)

Slika 14: Merjenje v 3D modelu: (a) koordinate; (b) razdalje.

4 ANALIZA IN RAZPRAVA

Položajna odstopanja na KT za slepi, priklepni in zaključeni fotogrametrični poligon so predstavljena v poglavju 3. Po pričakovanjih je točnost slepega poligona najnižja, saj so podane zgolj koordinate izhodišča poligona. Točnost položajev blizu izhodišča je v rangu nekaj centimetrov, se pa točnost niža z oddaljenostjo od izhodišča. Posebej moramo biti pozorni na točke, ki se pojavijo na manjšem številu slabo razporejenih fotografij. Po drugi strani pa manjše število projekcij ne pomeni nujno večjih odstopanj, tak primer je točka 502 v 3.2.1. Pomembno je, da so fotografije konvergentne, kar pomeni, da so zajete z različnih kotov, s tem zagotovimo ugodno geometrijo slikovnih žarkov.

Če so OT postavljene na skrajnih koncih poligona, to je na začetku za slepi poligon ter na začetku in koncu za priklepni in zaključeni poligon, samo število OT nima velikega vpliva na točnost točk v poligonu.

V splošnem je 4 do 5 nekolinearnih OT zadosti. Dodajanje OT na skrajnih delih poligona ne izboljša točnosti na KT. Pričakovano pa se točnost izboljša, če dodamo OT vzdolž poligona. V splošnem velja, da zgolj točne koordinate OT lahko omogočijo pridobitev točnih koordinat vzdolž poligona.

Gost oblak točk in 3D model sta zelo primerna za masovno določanje položaja, saj ima vsaka točka v oblaku svojo 3D koordinato. Gost oblak točk, predstavljen v 3.3, ima več kot 100 milijonov točk in sploh ne zajema celotne predavalnice. Točnost položajev točk v oblaku približno ustreza točnosti bližnjih KT.

4.1 Težave SfM pri obdelavi fotografij notranjih prostorov

Pri obdelavi fotografij, zajetih v notranjosti stavb, lahko ponovljivi vzorci povzročijo napačno ujemanje ključnih točk med fotografijami, ki so sicer zajete na različnih delih objekta. Dva od tovrstnih primerov sta vidna na sliki 15. Slika 15 (a) prikazuje situacijo, kjer je požarni evakuacijski načrt povzročil napačno slikovno ujemanje med fotografijama, zajetima na ločenih stopniščih. Posledično se v oblaku točk pojavi eno samo stopnišče namesto dveh, ki sta dejansko v stavbi. Dodatno je to stopnišče predstavljeno v treh delih (slika 15 (b) zgoraj), dejansko pa ga sestavljata le dva dela. Spodnji del slike 15 (b) prikazuje združeni predavalnici, kar je posledica postavitve enakega plakata v obeh predavalnicah.

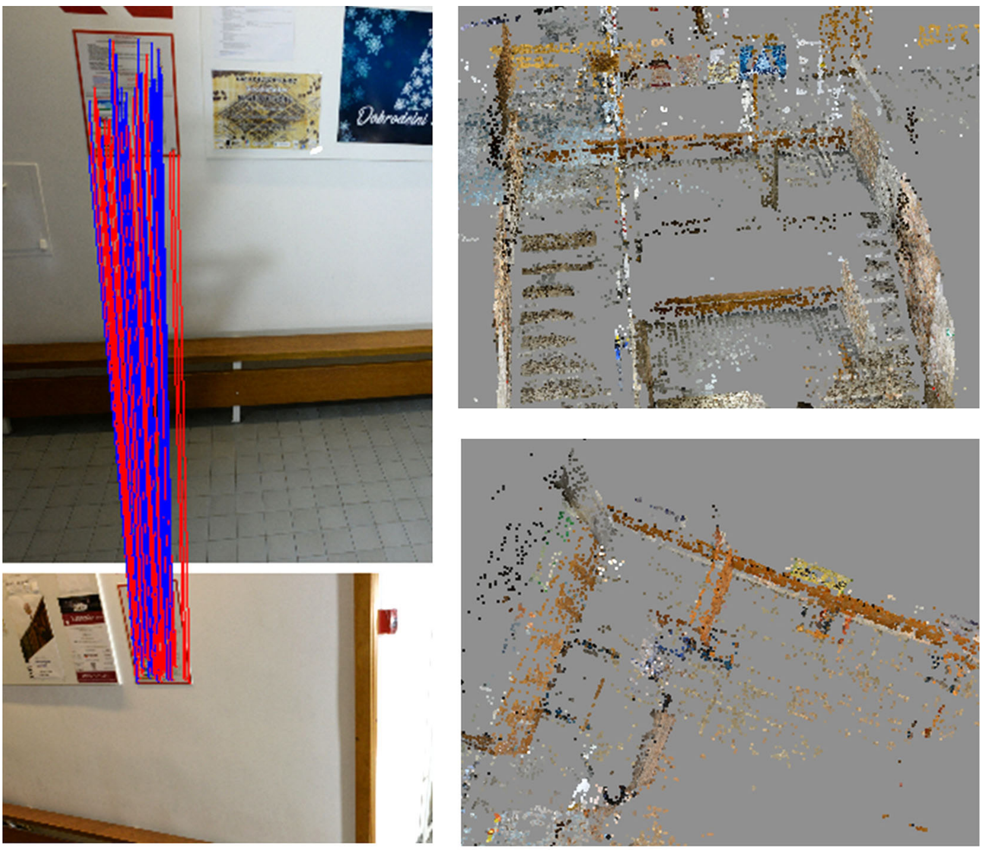

Slika 15: Težave s ponovljivimi vzorci: (a) ujemanje napačnih fotografij; (b) napačni modeli kot posledica.

Preostali vzorci, ki se pogosto ponovijo v stavbah: znaki za izhod v sili, ure, požarni alarmi ipd. Težave lahko odpravimo z maskiranjem kritičnih vzorcev na fotografijah. Postopek je pogosto tudi iterativen, saj ko zamaskiramo en problematičen vzorec, se lahko pojavi drug.

5 ZAKLJUČEK

Predlagana rešitev predstavlja geodetski poligon, le da smo namesto tahimetra uporabili fotoaparat. Tahimeter ali GNSS še vedno uporabimo za določitev položajev OT in KT, ostali terenski in pisarniški del pa temelji na fotogrametričnih postopkih.

Naši preizkusi so pokazali, da so položaji točk vzdolž poligona še vedno točni, četudi imamo več sto fotografij in smo nekaj 10 metrov oddaljeni od referenčnih točk. Tudi v slepem poligonu lahko dosežemo položajno točnost znotraj 2 cm na razdaljah do 40 m od izhodišča slepega poligona.

Če je izvedljivo, seveda priporočamo uporabo priklepnega ali zaključenega poligona, saj zagotavljata boljšo položajno točnost točk v poligonu in ponujata več možnosti preverjanja kakovosti. V skrajnih primerih uporabimo slepi poligon, ampak moramo biti previdni, saj se v slepem poligonu hitro pojavijo grobi pogreški, ki lahko ostanejo nezaznani. V splošnem lahko ponovljivi vzorci na fotografijah različnih delov objekta vodijo do napačnega slikovnega ujemanja. Da se temu izognemo, vzorce maskiramo.

Prostorska razporeditev OT zagotavlja dobro osnovo za določanje položaja točk v poligonu v vseh treh dimenzijah.

Predstavljeni preizkusi kažejo, da se fotogrametrični poligon lahko uporablja za določanje položaja točk v notranjosti objektov. Položaje OT določimo s tahimetrično izmero ali GNSS, za vse ostalo ne potrebujemo več običajne merske opreme. Ker GNSS ni mogoče uporabljati v notranjosti stavb ali pod zemljo, zelo omejeno pa v gosti vegetaciji in v bližini visokih stavb (tako imenovani urbani kanjoni), je kot rešitev za ta območja mogoč fotogrametrični poligon. Dodatno pa ne gre za točkovno določitev položaja, ampak za masovno pozicioniranje, kjer razmeroma enostavno pridemo do več milijonov georeferenciranih točk.

Gosti oblak točk z danimi položaji množice točk ni edini izdelek fotogrametrije. Teksturiran 3D model z velikim številom ploskev omogoča fotorealističen prikaz, kot je vidno na sliki 13. 3D model omogoča različne upodobitve, na primer pogled s poljubne perspektive in navidezne prelete. Lahko se uporablja tudi za različne izračune in merjenja količin, kot so razdalje, koti, površine, prostornine ipd.

Običajna geodetska izmera je omejena na določanje posameznih točk. Če je naknadno treba določiti koordinate točk v bližini predhodno izmerjenih točk, je potrebna ponovna terenska izmera. Prednost fotogrametrične izmere je v tem, da ni treba ponovno izvesti terenske izmere, ampak se lahko 3D položaj poljubne točke rekonstruira iz obstoječih fotografij. Pomanjkljivost fotogrametrične izmere je nezmožnost kontrole kakovosti izdelkov med samim zajemom, kajti vsi rezultati so dostopni šele po obdelavi fotografij v pisarni.

Po našem mnenju je fotogrametričen poligon lahko zelo uporaben tudi v naravnem okolju. S stališča fotogrametrične obdelave je v naravi zelo malo ponovljivih vzorcev, kar pomeni manjše težave v postopkih slikovnega ujemanja, ki so osnova za izračun orientacije fotografij. V gosti vegetaciji GNSS ne deluje ali pa deluje manj natančno, tahimetrični poligon pa zna biti zahteven ali celo neizvedljiv. V tovrstnih okoljih se fotogrametrični poligon pokaže kot zelo primerna in ugodna rešitev. To bo tema naših nadaljnjih raziskav.

Financiranje: Raziskavo je finančno podprla Javna agencija za znanstvenoraziskovalno in inovacijsko dejavnost Republike Slovenije (raziskovalna programa P2-0227 Geoinformacijska infrastruktura in trajnostni prostorski razvoj Slovenije in P2-0406 Opazovanje Zemlje in geoinformatika).

Literatura in viri:

Glej literaturo na strani 163.

Kozmus Trajkovski K., Urbančič T., Stopar B., Grigillo D. (2025). Fotogrametrični poligon za zajem podatkov v zaprtih prostorih. Geodetski vestnik, 69 (2), 148-179.
DOI: https://doi.org/geodetski-vestnik.2025.02.148-179

doc. dr. Klemen Kozmus Trajkovski
Univerza v Ljubljani, Fakulteta za gradbeništvo in geodezijo
Jamova cesta 2, SI-1000 Ljubljana
e-naslov: klemen.kozmus@fgg.uni-lj.si

prof. dr. Bojan Stopar
Univerza v Ljubljani, Fakulteta za gradbeništvo in geodezijo
Jamova cesta 2, SI-1000 Ljubljana
e-naslov: bojan.stopar@fgg.uni-lj.si

doc. dr. Tilen Urbančič
Geotočka d.o.o., Tehnološki park 24, 1000 Ljubljana
Univerza v Ljubljani, Fakulteta za gradbeništvo in geodezijo
Jamova cesta 2, SI-1000 Ljubljana
e-naslov: tilen.urbancic@fgg.uni-lj.si

doc. dr. Dejan Grigillo
Univerza v Ljubljani, Fakulteta za gradbeništvo in geodezijo
Jamova cesta 2, SI-1000 Ljubljana
e-naslov: dejan.grigillo@fgg.uni-lj.si